DIFFUSE LIGHT IN DENSE CLUSTERS OF GALAXIES. I.
R-BAND OBSERVATIONS OF ABELL 2029

JUAN M. USON[1]

National Radio Astronomy Observatory,[2] P.O. Box O, Socorro, NM 87801

STEPHEN P. BOUGHN[1]

Astronomy Department, Haverford College, Haverford, PA 19041

AND

JEFFREY R. KUHN

Department of Physics and Astronomy, Michigan State University, East Lansing, MI 48824

ABSTRACT

We have developed an observing technique that uses a CCD detector, multiple overlapping exposures, and a tesselating algorithm that allows us to do reliable differential photometry over a large (about $0°6$) field of view to a precision of 2×10^{-4} of the night-sky level, limited only by statistical noise.

We have measured the point-spread function of the telescope-detector combination out to 20' from the nominal pointing position. We have found that it is necessary to correct the data for the contamination from the extended halos of stars brighter than $m_R = 15.5$ in order to measure diffuse light at levels below $\mu \sim 26$, or about 1% of the average night-sky level.

We present R-band observations of the very dense cluster of galaxies Abell 2029. We detect an elliptical component of diffuse light—extended halo of the cD galaxy—with constant eccentricity of 0.9 that follows a de Vaucouleurs profile out to a distance of $425h^{-1}$ kpc [measured as $d = (r_{min} r_{max})^{1/2}$]. The integrated luminosity of the cD galaxy with this halo is $5 \times 10^{11} h^{-2} L_\odot$ (R band).

The ratio of the diffuse light to the total cluster light in the elliptical annulus between $d = 250h^{-1}$ kpc and $d = 425h^{-1}$ kpc is 0.10 ± 0.005, where the uncertainty comes mainly from the estimate of the contribution of the galaxies. We place an upper limit of 5% to the ratio of diffuse light to total cluster light in the elliptical annulus between $d = 425h^{-1}$ kpc and $d = 850h^{-1}$ kpc.

Subject headings: cosmology — galaxies: clustering — galaxies: intergalactic medium — galaxies: photometry

1. INTRODUCTION

Models for the evolution of galaxies in dense clusters emphasize the processes of mergers or cannibalism, tidal stripping, and accretion (see Dressler 1984 for a review). There is considerable uncertainty on the relative importance of these mechanisms. Merritt (1984) has argued that these processes are likely to be effective mostly during the initial collapse of the cluster, which makes it particularly difficult for observations to constrain their relative merit. The most direct probe of the contribution of tidal stripping is a measurement of the intergalactic cluster light. Indeed, numerical simulations suggest that between 10% and 70% of the initial mass in galaxies is released into the intergalactic medium as a diffuse component depending on the assumed tidal-stripping efficiency (Miller 1983). In addition, the mass of a cluster of galaxies that is inferred from its dynamics is much larger than implied from the luminosity of its galaxies; this is, of course, the "dark matter" problem. The matter stripped from the galaxies might contribute a significant part of the cluster mass and, conversely, even a large mass-to-light ratio for the dynamically required, but unseen, matter might provide an appreciable extra contribution to a diffuse component of cluster light.

Identifying such a low surface-brightness component of the cluster luminosity is a difficult task. Since a comparison between the surface brightness near the center of the cluster and that at some area beyond the cluster edge is required, we must observe a distant cluster or a large field of view. On the other hand, high spatial-resolution is needed in order to distinguish the diffuse component from a blend of galaxies at the faint end of the luminosity function, which mandates a small pixel size or choosing a nearby cluster. We have devised an observing technique using a CCD detector that allows the imaging of large fields at a level of about 0.02% of the night-sky brightness through multiple overlapping observations and a tesselating algorithm.

Previous searches for diffuse intracluster light have been inconclusive and have only provided weak limits on models. Oemler (1973) reported the detection of an extended envelope to the cD galaxy at the center of Abell 2670 which he traced out to about $400h^{-1}$ kpc (we write Hubble's constant as $100h$ km s^{-1} Mpc^{-1}). He estimated the contribution of this component to the total cluster light to be about 35%. A possible detection of diffuse light in the Coma cluster at a level of (diffuse light/total light) $\sim 30\%$ was reported by Thuan & Kormendy (1977), whereas Melnick, White, & Hoessel (1977) set an upper limit of 25%. More recently Gudehus (1989) has reported low limits on a possible component of diffuse light in the cluster A1689. However, it is likely that his "fitting and subtraction" procedure would have removed a component of diffuse light such as the one that we observe.

Abell 2029 has been extensively studied (Dressler 1981 and references therein; see also Malumuth & Krishner 1985). Dressler's estimate of the luminosity function shows the cluster to be one of the richest clusters in the sky with an estimated richness of 4.4 on Abell's scale. Dressler also measured a velocity dispersion of 1430 km s^{-1} for the galaxies located within 380″ (2 core radii) from the center of the cluster. Therefore this cluster is one of the densest in the sky, with a mass-to-light ratio of about 1000h in solar V-band units. The cluster is also observed to be a copious emitter of X-radiation (McHardy 1978).

2. OBSERVATIONS

We observed Abell 2029 with the No. 1 0.9 m telescope on Kitt Peak National Observatory on 1987 May 20. We chose the No. 3 RCA CCD camera because of its high well capacity and quantum efficiency. The 512 × 348 pixel detector was mounted at the f : 7.5 Cassegrain focus with its long dimension aligned with the east-west direction. The pixels were square, 0″.86 on a side, adequate to the 1″.3 to 1″.4 seeing conditions. We obtained two sets of partially overlapping frames along the east-west direction (nine frames) and north-south direction (seven frames). The overlap between neighbors was about one-half of a frame and both strips were centered on the dominant cD galaxy located at the center of the cluster. In order to minimize the effects of a systematic variation of the sky background other than a change in the sky level (which we eliminate through our data processing scheme discussed below) the frames were not taken sequentially. Instead, after the central picture was taken, we alternated exposures on both sides of the center of each strip. We interspersed the observations of the cluster with those of 16 " blank " sky positions located between 0°.5 and 1° of the cluster center. All of these exposures lasted 5 minutes which resulted in similar contributions of photon shot noise and detector readout noise. A nearby SAO star was observed for two successive 3 second exposures every three long exposures in order to monitor extinction. Thus, the full observing sequence was center, blank, 210″ east, SAO, SAO, blank, 210″ west, blank, SAO, ..., center, blank, 160″ north, SAO, SAO, blank, 160″ south, ...

We observed a set of standard stars from Landolt's *UBVRI* secondary calibration list (Landolt 1983) in the range m_R: 10–12 with $(B−V)$ colors in the range from 0.0 to 2.0. The derived calibration constants agreed to within $\leq 0.02m_R$ after correction for a best-fit secant-law extinction. We estimate that our absolute calibration errors are less than 5%.

We measured the light-scattering properties of the telescope and detector optics through observations of several bright and isolated stars. In order to determine the wings of the point-spread function (PSF) we observed blank sky in the vicinity of such stars at angular distances up to 2200″ from them. We have collected an extensive set of data on the PSF of this system with observations made in 1987 May 20–21, 1988 May 8–15, and 1989 January 6–8.

Finally, standard out-of-focus exposures of a " white spot " on the telescope dome were used to construct a standard " dome-flat " picture.

3. DATA REDUCTION

3.1. *Zeroth-Order Processing*

At the telescope, the raw CCD frames were corrected for the bias level and trimmed to a useful size of 316 × 508 pixels using standard KPNO software. This subtracts each picture's overscan and corrects for pixel-to-pixel variations of the zero-point offset of the signal levels using a null exposure " bias " frame. The pictures were then written to standard FITS tapes and further processing was done using our own software.

3.2. *Calibration of Pixel-to-Pixel Gain Variations*

It is well known that although CCD detectors are linear over a large dynamic range, they show significant pixel-to-pixel gain variations. A first-order correction is routinely accomplished through division by " dome-flats," which leaves residual gain variations of about 1%. In order to improve on this level, we generated a " sky-flat " picture in the following way. The exposures of " blank " areas, corrected by the " dome-flat " picture, were purged of objects using a robust 2.5 σ filter (five iterations). The standard deviation per pixel, σ, is about 5% of the night-sky level. This procedure leaves behind the extended, low-level envelopes of the objects in the frames. After finding the centroid and rms radius of each object, the radii were scaled by a factor of 5 and all pixels contained inside these areas were dropped. The resulting frames were scaled to unity average and subsequently averaged to produce the sky-flat frame. This frame is equivalent to a 60 minute exposure of blank sky. This image was clean of residual ghost image structures to better than 0.1%. We found no evidence of fringing at the same level.

The sixteen cluster frames were divided by the sky flat and scaled to correct for extinction using the secant law determined from the observation of standard stars.

3.3. *Tesselation of the Cluster Frames*

The calibrated cluster frames were then filtered as described above. The robust 2.5 σ filtering and subsequent enlargement of the cut-out region of the object pixels produced two sets of pictures: " object " pictures and " background " pictures. The cut-out radius was chosen to satisfy two conflicting requirements: the need to avoid contamination from the outskirts of objects without losing two many pixels. It results in about 60% of the pixels being designated as objects and thus removed from the diffuse light analysis in the central region of the cluster.

The " object " pictures were cross-correlated to register the frames spatially. Comparison of the peak in the two-dimensional cross-correlation with offsets found from fitting the centroids of stars in the overlapping areas shows that our offsets are accurate to better than one-half pixel, quite sufficient for our purposes.

The mean sky level was $m_R = 21.0$ arcsecond^{-2} and varied by up to ± 33% throughout the night. We assume this to be mostly a variation in the DC level due to changes in airglow and correct for it as follows. We use the overlapping areas of any pair of " background " frames to determine an offset between the two frames in the least-squares sense. The minimization leads to an offset value that, in the absence of gradients, would be equal to the difference of the average sky levels in the overlapping areas of the two pictures. Because some pixels might have been " blanked " on one picture while the corresponding ones might not be deleted in another frame, a gradient (perhaps induced by the flat-fielding procedure) might bias the estimate of the offset. In order to avoid such bias, only corresponding pixels that are defined in both frames are used to determine the offset between any pair of images.

The observations of the nearby SAO star were used to check the reproducibility of the photometry. This was independently
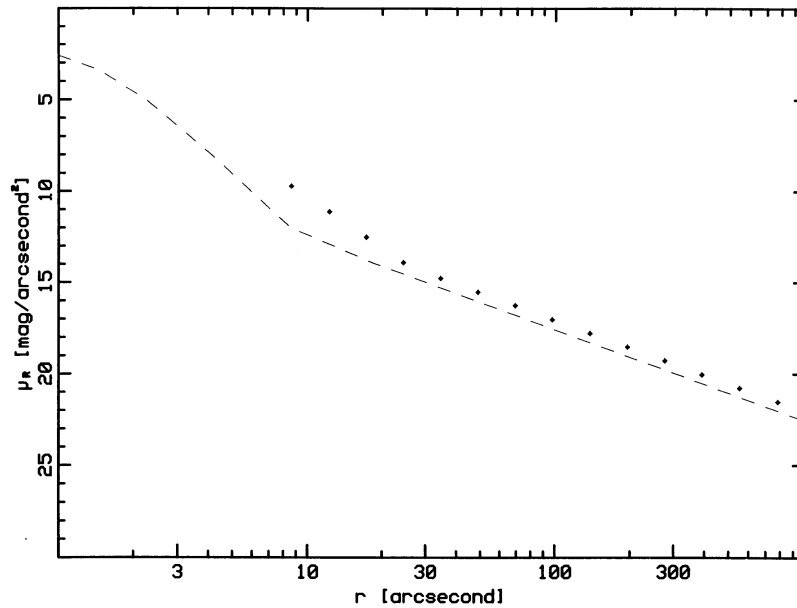
FIG. 2.—Our PSF function is plotted against the canonical PSF function as determined by King (1971). The crosses represent our measurements using the mosaic observations of several stars as bright as $m_R = 3.5$.

checked by comparing the stars in the overlap region of consecutive cluster exposures. The agreement was excellent (0.00 $\pm$ 0.01m_R) until the third exposure of the north-south strip (0.08 $\pm$ 0.10m_R) when thin clouds must have appeared. The night progressively deteriorated from then on. These data, although cosmetically pleasant (see Fig. 1 [Pl. 1]) have been excluded from the statistical analysis described below. Because some sky positions were observed on more than two pictures, this straightforward procedure does not, in general, allow the so-determined offsets to "close."

A better solution is accomplished by an algorithm that uses all the data in order to produce a global least-squares determination of the offsets (Boughn & Kuhn 1986). The sky brightness, $S_i(r)$, observed at any given location r with frame i is given by

$$S_i(r) = b(r) + a_i , \tag{1}$$

where $b(r)$ is the true sky brightness and a_i is the offset associated to frame i. We define for each picture a "window" function $W_i(r)$ which is unity if the pixel is "good" in that frame and zero otherwise.

The global determination of the offsets a_i is then given by a minimization (in the least-squares sense) of the "errors" given by the multiple determination of the sky level at each given position. That is we minimize the expression

$$\sum_r \sum_i \{S_i(r) - W_i(r)[b(r) + a_i]\}^2 \tag{2}$$

with respect to the observed sky brightness, $b(r)$, and the offsets, a_i.

The minimization of this quadratic equation yields a set of coupled linear equations

$$C_{ij} a_j = \sum_r [S_i(r) - \langle S(r) \rangle_W] W_i(r) , \tag{3}$$

where the coefficients C_{ij} are given by

$$C_{ij} = N_i \delta_{ij} - \sum_r \frac{W_i(r)W_j(r)}{N(r)} , \tag{4}$$

with

$$N(r) = \sum_i W_i(r) \tag{5a}$$

and

$$\langle S(r) \rangle_W = \sum_i \frac{S_i(r)W_i(r)}{N(r)} . \tag{5b}$$

$N(r)$ is the number of actual measurements of the sky brightness at position r and $\langle S(r) \rangle_W$ is its average value (which is not our best estimate of the sky brightness as it does not contain the actual offsets).

The coefficient matrix C_{ij} is symmetric and singular. This is to be expected as the problem is invariant under a global intensity offset, i.e., it has to be degenerate. We solve the equations in (4) with the constraint that the average sky level does not change, i.e., that

$$\sum_i a_i = 0 . \tag{6}$$

Figure 1 shows our mosaic of A2029.

3.4. Correction of Contamination from Stars

The PSF was determined by generating a mosaic of our observations in the same way as described above. We adopted as the reference level the average level from $r = 800''$ to $r = 1360''$ and analyzed the mosaic assuming circular symmetry with the level in each ring given by the peak of a Gaussian fit to the pixel intensity distribution in the manner discussed in the next section. The resulting PSF is shown in Figure 2 and shows the extended $1/r^2$ aureole first described by King (1971) in his study of the universal PSF. We believe our PSF to be accurate to about 5% out to a distance of about 500".

The robust filtering scheme described above (§ 3.2) removes objects brighter than $m_R = 21.0$ but leaves behind the extended $1/r^2$ halos of bright stars and galaxies. We photometered all objects within 20' of the cluster center that were brighter than

PLATE 1

Right Ascension (1950.0)

Declination (1950.0)
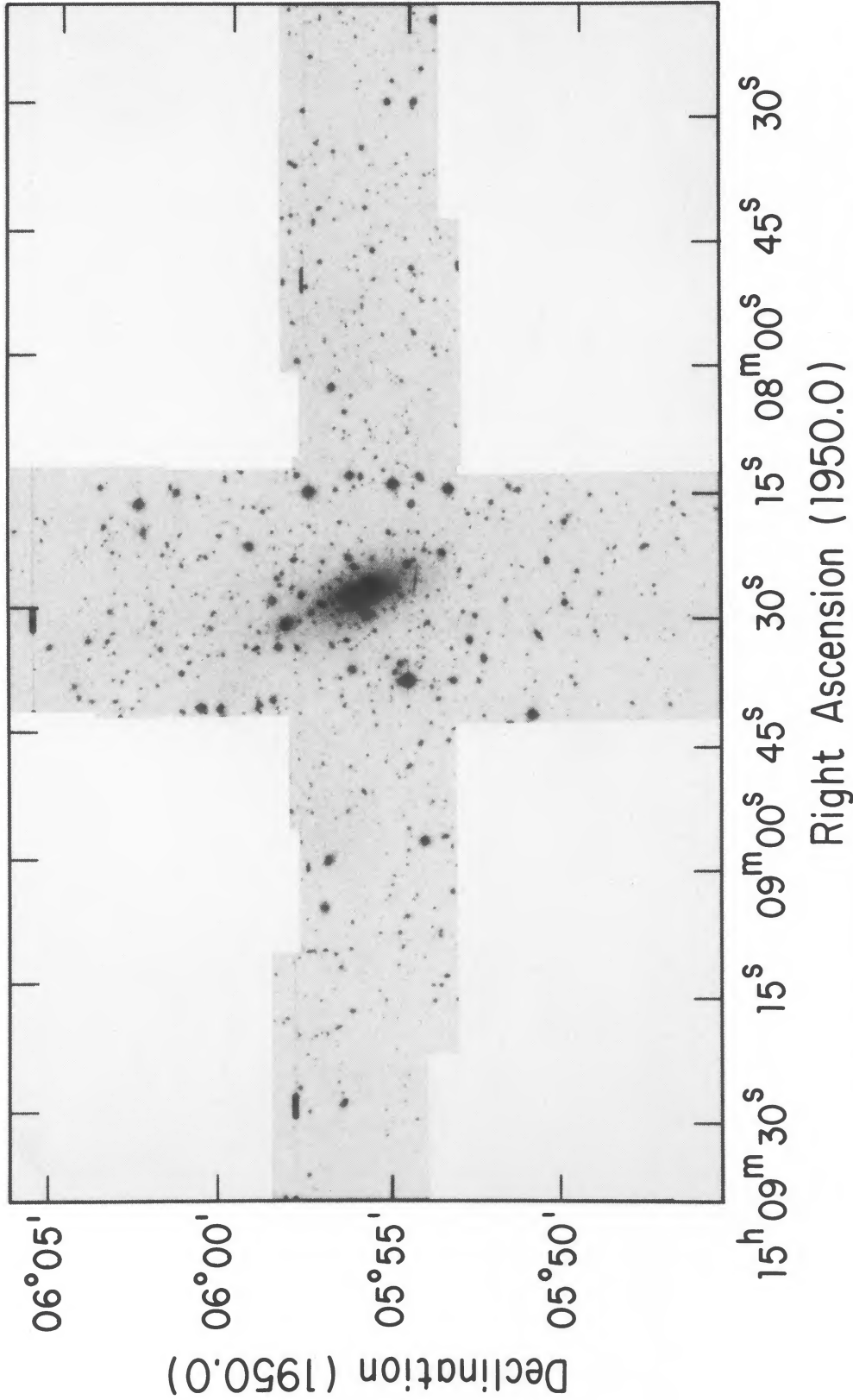
Fɪɢ. 1.—A photographic reproduction of the tesselated CCD data. The cross pattern is centered on the cD galaxy in Abell 2029. The intensity scale is linear in photographic density where $\mu_R = 20.4$ is black and $\mu_R = 21.6$ is white.

Usᴏɴ, Bᴏᴜɢʜɴ & Kᴜʜɴ (see 369, 48)

$m_R = 15.5$. Their extended halos were computed using our measured PSF and subsequently subtracted from the data pixel by pixel. It is notable that, even though the data were not obtained in a crowded stellar field, a few stars can have an important effect on measurements of diffuse light. We also checked the level of contamination from bright stars by evaluating the effect of all SAO stars located within a few degrees of the cluster center and found their contributions to be negligible. Finally, we also computed the scattered light from the cD galaxy itself and corrected the data accordingly (§ 4.2).

4. ANALYSIS

4.1. General Considerations

The diffuse halo of the cD galaxy in A2029 is readily apparent in the mosaic picture. Figure 3 shows that the isophotes that characterize this halo are well described by a set of concentric ellipses with roughly constant eccentricity, $e = 0.9$ or an axis ratio 2:1, which holds as far from the cluster center as the contours can be traced. In this inner region our R-band photometry is consistent with the V-band photometry of Dressler (1981) within the estimated errors with a color of $V - R = 0.8$. The galaxy counts of Dressler (1978) indicate that the structure of the cluster maintains its elliptical configuration out to several cluster core radii. We will assume that any extension of the diffuse halo maintains this constant eccentricity. The analysis described in the next section supports this assumption.

We have determined the luminosity function for the galaxies located within two core radii of the cluster center. The results are in good agreement with those of Dressler (1978).

4.2. A Statistical Determination of the Diffuse Light

The isophotal contours in Figure 3 extend out to $51'' \times 105''$ from the cluster center. Beyond this range the noise in the image renders the interpretation of the contours meaningless. A straightforward approach to separating the observed light into a contribution from galaxies and what we will call a background contribution is to remove all "object" pixels and use the remaining ones to compute the mean intensity distribution $i(r)$. Clearly such an analysis suffers from the inevitable, possibly systematic, variation in our object (galaxy) detection threshold, which could very well depend on the distance to the cluster center. The cluster contains many faint objects which bias such determination toward higher values whereas choosing the lowest or median values in any area might also bias the estimate.

We have used a statistical approach which uses the data in an objective way. The pixels in the 11 frames (the nine frames of the EW strip plus the first two frames in the NS strip) were grouped in concentric elliptical bins of axis ratio 2:1 and widths ranging from 5 pixels to 120 pixels. Figure 4 shows a composite of 42 such pixel-intensity distributions with semiminor axes ranging from $14''$ to $790''$. Each histogram results from a convolution of the true sky intensity distribution—objects plus background light—in a given elliptical bin with a distribution that characterizes the measurement noise. This noise is a combination of photon shot noise and CCD readout noise which, by the central-limit theorem, results in an approximately Gaussian noise distribution. We argue below that the positions of the peaks of these curves indicate the level of the diffuse background and Figure 4 shows its variation with distance from the cluster center. The central pixels of bright objects have large intensities and therefore have no effect on the determination of the diffuse light. It is of some concern that the extended tails of such objects as well as faint objects might bias the estimate of the diffuse light. We address this problem below.

Let us describe the light distribution in Figure 4 in a sta-
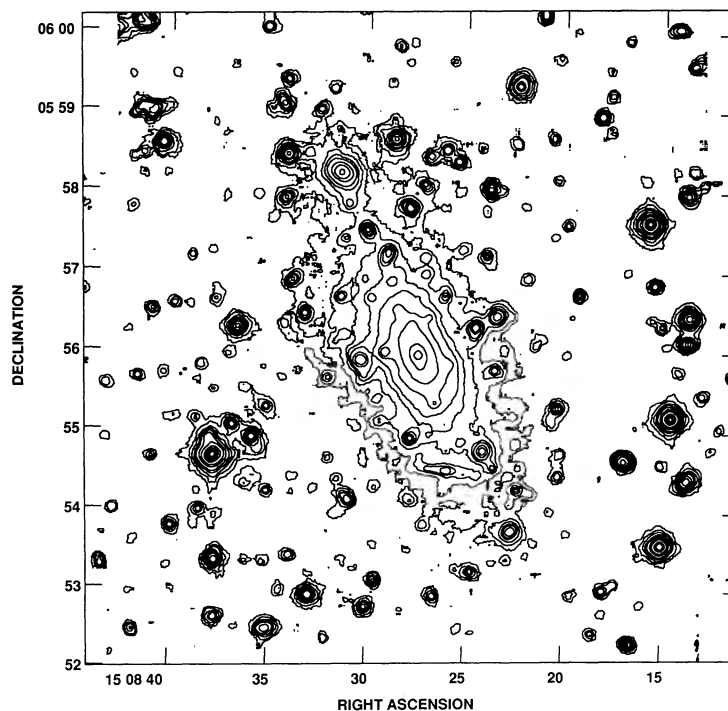
FIG. 3.—A contour map of the central region of the tesselated image shows the cD galaxy with its extended envelope of diffuse light. Contour levels are respectively 1.5%, 3%, 5%, 8%, 11%, 20%, ... of the average night-sky level.
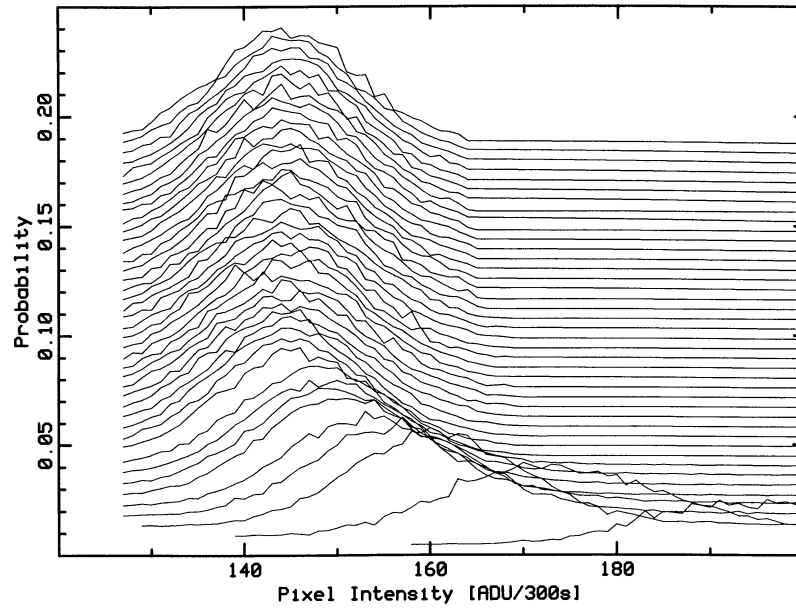
FIG. 4.—A plot of histograms of pixels in 42 elliptical annuli centered on the cD galaxy. The lowest nine correspond to annuli with (minor axis) width of 10 pixels, whereas for the upper 33 the width was 25 pixels. The lowest curve is the normalized probability distribution for data near (minor axis) distance 14″ and the upper curve corresponds to data in the elliptical annulus with semiminor axis length about 790″. The histograms are displaced vertically to improve visibility.

tistical sense. The intensity, i, in any given pixel contained in (elliptical) bin α results from a combination of the emission from the objects, airglow, a diffuse intergalactic component as well as any population of faint, unresolved, background sources. The set of pixel-intensity distributions in Figure 4 can be described by $P_{i\alpha}$, the probability that a pixel in bin α has an intensity in bin i, which can be expressed as

$$P_{i\alpha} = N_\alpha W_i + (1 - N_\alpha)V_i \,, \tag{7}$$

where N_α is the probability that an object contributes to a pixel in bin α and W_i and V_i are the convolutions of the object intensity distribution, O_i, and the background distribution, B_i, with the noise distribution, R_i, i.e.,

$$W_i = O_i * B_i * R_i \,, \tag{8a}$$

and

$$V_i = B_i * R_i \,, \tag{8b}$$

where W_i also contains the distribution of background intensity as objects always exist on top of the background emission. R_i is due to the combination of any source of noise and is therefore also a convolution of the Poisson distribution due to shot noise and the Gaussian distribution of CCD readout noise. The width of the histograms is within 8% of that expected from our estimate of the noise.

Since the average number of photons per pixel is large, about 1300 are from the night sky alone, and the readout noise is about equal to the photon shot noise, R_i is well represented by a Gaussian distribution. The distribution is narrow, $\delta i/i \approx 0.05$ so that it is adequate to approximate R_i by a Gaussian distribution of fixed width. It is in this limit that equations (8) are exact, i.e., the distributions V_i and W_i are given by true convolutions. The approximation breaks down for the large intensities associated with objects and would also break down with large variations of the sky background level as the width of the Gaussian noise distribution depends on the measured intensity level. The airglow variations were not large and, as we

discussed above, the pixels containing bright objects have no effect on the determination of the diffuse component as the object intensity distribution is very broad and shallow.

Let us assume that the background distribution depends only on the elliptical bin α. Let us further assume that its width is much smaller than that of the noise distribution R_i which is supported by the comparison of the actual width of the histograms with the expected width of R_i. It is in this case adequate to describe B_i by a Dirac distribution,

$$B_i = \delta(i - b_\alpha) \,, \tag{9}$$

where b_α is the value of the background intensity in bin α. Substitution in equation (7) leads to

$$P_{i\alpha} = N_\alpha O_i R_i(i - b_\alpha) + (1 - N_\alpha)R_i(i - b_\alpha) \,. \tag{10}$$

To the extent that the object intensity distribution is assumed to be independent of position in the cluster, only $3\alpha + i$ parameters, O_i, b_α, N_α, and σ_α (the width of the noise distribution in bin α) need to be determined from $i \times \alpha$ measurements in the set of intensity distributions and the problem is in general overconstrained. The assumption of the independence of O_i on radial bin suggests that bright objects be excluded from the analysis and that the luminosity profiles of the objects do not overlap. Otherwise this overlap could have a dependence on the density of objects, N_α. This assumption is not overly restrictive since as multiple objects overlap they blend into a diffuse background and their description as individual objects becomes irrelevant.

The $3\alpha + i$ unknowns could, in principle, be determined from a least-squares fit to the data. However, recovering the object intensity distribution, O_i, involves its deconvolution from the noise distribution, R_i, which is numerically difficult with noisy data. We have used a numerically simpler solution which, although it does not allow O_i to be computed, retrieves enough information to determine the diffuse light.

It is interesting to note that there is a mathematical ambiguity in the solution of equation (7) such that if a solution

is described by $\{N_\alpha, O_i, R_i,$ and $B_i\}$, the solution $\{cN_\alpha, O_i/c +$ $(1 - 1/c)\delta(i), R_i,$ and $B_i\}$ also describes the data. The scaling has no physical consequence as it involves the counting of an extra contribution $(1 - 1/c)$ of objects of zero intensity. The mathematical ambiguity, however, illustrates the difficulty involved in deconvolving the component distributions from the measured data.

Since the information on the distribution of objects that can be obtained with this technique is quite limited (as interesting objects are multiple-pixel entities) and the determination of the background intensity distribution is not affected by the scaling relation, we proceeded to determine the background component in the following, straightforward, way.

We have found that fitting any of the histograms in Figure 4 to a Gaussian function yields a mean which is identical to the values of b_α from the above least-squares solution, provided that the fit excluded bins with intensities far above that of the peak of the Gaussian function. We only used those bins with intensities below $b_\alpha + \sigma_\alpha$ and, furthermore, excluded those bins with occupancy less than 5% of that of the peak intensity in order to minimize a bias due to small number statistics.

The Gaussian fitting procedure is potentially sensitive to a bias introduced by the extended envelopes of galaxies and stars. We investigated the extent of this problem by performing the same procedure on a model cluster generated from a Schechter (1976) luminosity function with galaxy profiles taken from Binggeli, Sandage, & Tarenghi (1984) in addition to a diffuse radially dependent background and the noise appropriate to our airglow level. This analysis demonstrated that the determination of the diffuse background was biased by the extended profiles of bright galaxies (i.e., $M < M^*$), although the contamination was relatively small, typically about 0.2% of the night-sky level at a distance of one core radius from the cluster center. This analysis also indicated that the bias was eliminated by excluding a guard band around bright objects in the way described in § 3.2.

The CCD frames were therefore subject to a 2.5 σ robust filter (again 5 iterations) and again 3 or more contiguous, non-colinear pixels were designated as "objects." After determining the centroids and rms radii, two sets of pictures were generated by enlarging the radius of the blanked regions by factors of 3.5 and 5. Pixel intensity distributions were then recomputed for each set of images with the flagged pixels removed from consideration. The fitted values of the b_α were different, as expected, from those obtained above; although no significant differences were found between both sets of pictures, in agreement with the Monte Carlo predictions. Thus the pictures with the 3.5 times guard-band have been used for the remaining analysis.

Gaussians were fitted to the histograms in each elliptical bin with the restriction that the fitted function areas are normalized to a value appropriate to a distribution truncated beyond 2.5 standard deviations (since the empirical distributions have been truncated at 2.5 σ). This restriction relates the width and amplitude of the Gaussian and reduces the number of free parameters to two—the variance and the mean. We found that this amplitude-scaling made the fitted values insensitive to our high-end cutoff.

The scattered light from the cD and its envelope was computed and removed by deconvolving the PSF determined in § 3.4.

Table 1 shows the intensity of the diffuse light as a function of distance to the center of the cD galaxy measured along the

TABLE 1
INTENSITY OF DIFFUSE LIGHT

Minor Axis Distance	Intensity $(10^{-20}\text{ ergs s}^{-1}\text{ cm}^{-2}\text{ sr}^{-1}\text{ Hz}^{-1})$
3.2	1027 ± 15
4.0	782 ± 24
4.7	642 ± 24
5.6	546 ± 21
6.5	469 ± 21
7.3	394 ± 18
8.2	346 ± 12
9.0	315 ± 9
9.9	273 ± 7
10.8	257 ± 6
12.0	210 ± 4
14.3	164 ± 2
18.1	113 ± 1
24	67.2 ± 0.9
32	39.5 ± 0.6
41	27.8 ± 0.6
50	20.3 ± 0.5
60	13.1 ± 0.3
74	7.61 ± 0.21
94	4.36 ± 0.18
114	2.51 ± 0.15
139	1.49 ± 0.15
167	0.87 ± 0.15
207	0.48 ± 0.15
253	0.48 ± 0.15
312	0.00 ± 0.15
388	-0.18 ± 0.12
475	0.00 ± 0.12
584	-0.09 ± 0.09
710	0.06 ± 0.09
884	0.09 ± 0.09

NOTES.—The quoted errors are statistical only. The transformation from R-band magnitudes to physical units: $\mu_R = 21.0$ corresponds to $5.1 \times 10^{-18}\text{ ergs s}^{-1}\text{ cm}^{-2}\text{ sr}^{-1}\text{ Hz}^{-1}$ was taken from Johnson 1966.

minor axis of the elliptical bins. At (minor axis) distances between $260''$ and $900''$ the intensity is constant with an rms scatter about the mean of $30.6m_R$ which corresponds to 2×10^{-4} times the average night-sky level. This value is consistent with that expected from shot noise and CCD readout noise.

Finally, we also analyzed the data binned in circular rings. We found that for all radial bins inside $260''$ the fitted width to the intensity histograms exceeded that of the corresponding elliptical bin. This is consistent with our expectation that the diffuse light has significant eccentricity as far away as it is detected.

5. DISCUSSION

5.1. cD Profile

The data of Table 1 were fitted to a de Vaucouleurs (1948) profile

$$I(r) = Ae^{-(r/r_0)^{1/4}}, \tag{11}$$

and the result is plotted in Figure 5. The fit has a $\chi^2 = 19.4$ for 25 degrees of freedom. There is no evidence for a departure from the de Vaucouleurs law as far as we can trace the diffuse envelope. Whether this diffuse light is called the cD envelope or diffuse intergalactic light is a matter of semantics; it is a diffuse component which is distributed with elliptical symmetry about the center of the cluster potential.

Also plotted in Figure 5 (*dashed curve*) are the results of the diffuse light determination without correcting the frames for
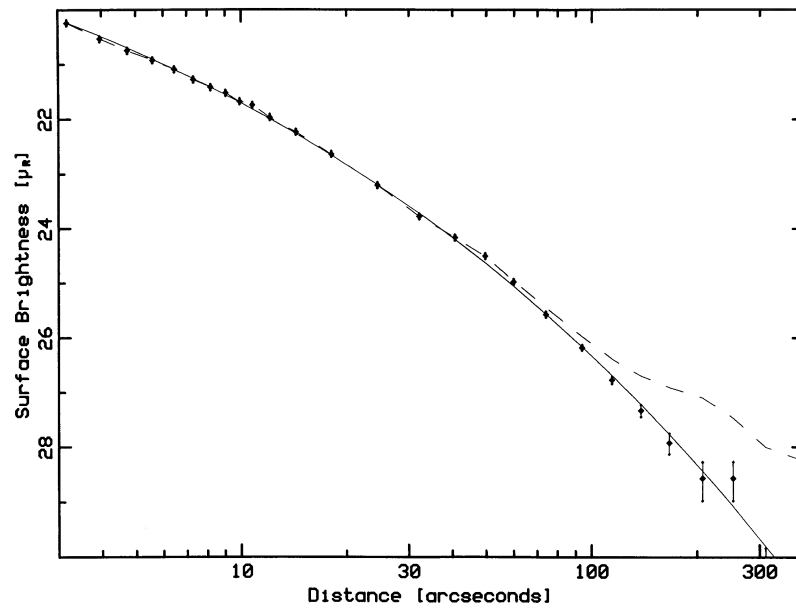
FIG. 5.—A fit of the diffuse light (measured in elliptical bins of constant axis ratio 2:1) to a de Vaucouleurs profile. The horizontal axis is the semiminor axis length of the bins. The dashed curve shows the light levels before correcting for the extended envelopes of bright stars (see text).

the extended halos of stars brighter than $m_R = 15.5$. It is evident from this curve that such corrections are necessary in order to determine diffuse light at levels below $\mu_R = 26$, or about 1% of the average night-sky level. About half of this contamination results from light scattered beyond 1'. If the broad $1/r^2$ wing to the PSF of telescopes is indeed universal, as emphasized by King (1971), this type of correction is critical to any observations of faint diffuse light.

5.2. Total Light

If the diffuse light continues to follow a de Vaucouleurs profile (or cuts off at large distances), the total cD light is easily calculated by integrating the analytic function. Assuming constant eccentricity, the total light of the cD and its envelope correspond to $m_R = 12.0$. Let us point out that 92.3% of the derived total light lies inside the ellipse with minor axis of 260", which marks the limit of our detection of the diffuse light. When K corrected ($q_0 = 0.5$), this implies a total R-band luminosity of $5 \times 10^{11}h^{-2} L_\odot$.

We estimated the total cluster light by adding up the total light in elliptical bins after excising stars brighter than $m_R = 17$. We estimated the contribution of the remaining foreground stars and background galaxies using nearby blank fields. The resulting curve of growth was well behaved and indicated a total cluster luminosity of $(2.2 \pm 0.5) \times 10^{12}h^{-2} L_\odot$ extending out to 700" on the minor axis. Thus 23% of the cluster light is emitted by the cD galaxy and its envelope. Table 2 shows the ratio of diffuse light (including that of the cD) to total light for several elliptical bins.

5.3. Mass-to-Light Ratios

Also listed in Table 2 are estimates of the R-band mass-to-light ratios for the diffuse light in these elliptical bins. The projected mass in these bins was computed for the isotropic King profile with core radius $r_c = 0.2h^{-1}$ Mpc and a line-of-sight velocity dispersion of 1430 km s^{-1} (Dressler 1981). Although estimates of the total mass of a cluster made in this way are sensitive to the detailed distribution of matter, projected mass densities from 0.5 to 3 core radii are far less dependent on the distribution of dark matter and, in particular, on the core radius (Bailey 1982; Boughn & Uson 1986).

Although the King model is spherically symmetric, the projected mass was computed in elliptical bins for comparison with the diffuse light. A proper dynamical model should take into account the eccentricity. For comparison, the R-band mass-to-light ratio of an M8 dwarf is $M/L \approx 690$ whereas it is $M/L \approx 4400$ for the extreme dwarf VB10 (Greenstein, Neugebauer, & Becklin 1970), where we have assumed that the mass of an M8 dwarf is 0.1 $M_\odot$ and that of VB10 is 0.085 $M_\odot$. This implies that the dark matter, if it is smoothly distributed, cannot consist primarily of main-sequence stars.

5.4. Dwarf Galaxies

The statistical method discussed in § 4 cannot distinguish diffuse light from the blend of a population of dwarf galaxies. We estimate that all galaxies brighter than $m_R = 21.3$ are eliminated by our filtering procedure. This limit corresponds to 4.5 mag below the characteristic M^* of A2029. Using our derived

TABLE 2

LUMINOSITY AND MASS-TO-LIGHT RATIO

Minor Axis Distance	Diffuse Light ($L_\odot$ h^{-2})	Total Light ($L_\odot$ h^{-2})	Diffuse Light/Total Light	Mass/Diffuse Light
0"–260"	4.6×10^{11}	1.1×10^{12}	0.41	$1500h$
155–260	3.8×10^{10}	3.7×10^{11}	0.10	$7800h$
260–525	$\leq 2.8 \times 10^{10}$	6.2×10^{11}	≤ 0.05	$18000h$

luminosity function we find that no more than 4% of the total cluster light could be due to galaxies fainter than the cutoff. Furthermore, less than one-half of this light falls below the cutoff intensity of the fitting procedure discussed in § 4. We conclude that less than 2% of the cluster light can possibly contaminate our measurement of diffuse light.

6. CONCLUSIONS

Using a new statistical approach we have measured the diffuse light component in A2029 beyond one cluster core radius. We find that the profile follows the de Vaucouleurs law out to a distance $d = 425h^{-1}$ kpc where we evaluate the distance to an elliptical annulus as $d = (r_{min} r_{max})^{1/2}$. The integrated luminosity with this halo is $5 \times 10^{11} h^{-2} L_\odot$. This is possibly one of the largest and most luminous galaxies in the universe.

Upper limits on diffuse light beyond one core-radius constrain the make-up of the dynamically inferred cluster mass. If the dark matter in this cluster is smoothly distributed, it cannot be composed of main-sequence stars.

Attempts to measure diffuse light can be seriously affected by stellar light scattered beyond $\sim 1'$. Figure 5 demonstrates the importance of this effect at low light levels, $\mu_R \geq 26$.

REFERENCES

Bailey, M. E. 1982, MNRAS, 201, 271
Binggeli, B., Sandage, A., & Tarenghi, M. 1984, AJ, 81, 64
Boughn, S. P., & Kuhn, J. R. 1986, ApJ, 309, 33
Boughn, S. P., & Uson, J. M. 1986, in Continuum Radio Processes in Clusters of Galaxies. ed. C. P. O'Dea and J. M. Uson (Green Bank: NRAO), p. 255
de Vaucouleurs, G. 1948, An. d'Ap, 11, 247
Dressler, A. 1978, ApJ, 222, 23
———. 1981, ApJ, 243, 26
———. 1984, ARA&A, 22, 185
Greenstein, J. L., Neugebauer, G., & Becklin, E. E. 1970, ApJ, 161, 519
Gudehus, D. H. 1989, ApJ, 340, 661

Johnson, H. L. 1966, ARA&A, 4, 193
King, I. R. 1971, PASP, 83, 199
Landolt, A. U. 1983, AJ, 88, 439
Malumuth, E. M., & Kirshner, R. P. 1985, ApJ, 291, 8
McHardy, I. 1978, MNRAS, 184, 783
Melnick, J., White, S. D. M., & Hoessel, J. G. 1977, MNRAS, 180, 207
Merritt, D. 1984, ApJ, 276, 26
Miller, G. E. 1983, ApJ, 268, 495
Oemler, A., Jr. 1973, ApJ, 180, 11
Schechter, P. 1976, ApJ, 203, 297
Thuan, T. X., & Kormendy, J. 1977, PASP, 89, 466